Carcinogenesis, 2021, Vol. 42, No. 8, 1100–1109

doi:10.1093/carcin/bgab050
Advance Access publication 12 June, 2021
Original Article

ORIGINAL ARTICLE

Constitutive Hedgehog/GLI2 signaling drives extracutaneous basaloid squamous cell carcinoma development and bone remodeling

Marina Grachtchouk[1], Jianhong Liu[1], Mark E.Hutchin[1], Paul W.Harms[1,2,3,4], Dafydd Thomas[2,4], Lebing Wei[1], Aiqin Wang[1], Donelle Cummings[1], Lori Lowe[1,2], Jonathan Garlick[5], James Sciubba[6], Arul M.Chinnaiyan[2,3,4,7], Monique E.Verhaegen[1,*] and Andrzej A.Dlugosz[1,4,8,*]

[1]Department of Dermatology, University of Michigan, Ann Arbor, MI, USA, [2]Department of Pathology, University of Michigan, Ann Arbor, MI, USA, [3]Michigan Center for Translational Pathology, University of Michigan, Ann Arbor, MI, USA, [4]Rogel Cancer Center, University of Michigan, Ann Arbor, MI, USA, [5]Division of Cancer Biology and Tissue Engineering, Tufts University School of Dental Medicine, Boston, MA, USA, [6]The Milton J. Dance Head and Neck Center, Greater Baltimore Medical Center, Baltimore, MD, USA, [7]Department of Urology, University of Michigan, Ann Arbor, MI, USA and [8]Department of Cell and Developmental Biology, University of Michigan, Ann Arbor, MI, USA

*To whom correspondence should be addressed. Tel: +1 734 647 9482; Fax: +1 734 763 4575; Email: dlugosza@umich.edu
Correspondence may also be addressed to Monique E. Verhaegen. Tel: +1 734 615 5209; Fax: +1 734 763 4575; Email: moniquev@umich.edu

Abstract

Uncontrolled activation of the Hedgehog (Hh) signaling pathway, operating through GLI transcription factors, plays a central role in the pathogenesis of cutaneous basal cell carcinoma and contributes to the development of several malignancies arising in extracutaneous sites. We now report that *K5-tTA;tetO-Gli2* bitransgenic mice develop distinctive epithelial tumors within their jaws. These tumors consist of large masses of highly proliferative, monomorphous, basaloid cells with scattered foci of keratinization and central necrosis, mimicking human basaloid squamous cell carcinoma (BSCC), an aggressive upper aerodigestive tract tumor. Like human BSCC, these tumors express epidermal basal keratins and differentiation-specific keratins within squamous foci. Mouse BSCCs express high levels of *Gli2* and Hh target genes, including *Gli1* and *Ptch1*, which we show are also upregulated in a subset of human BSCCs. Mouse BSCCs appear to arise from distinct epithelial sites, including the gingival junctional epithelium and epithelial rests of Malassez, a proposed stem cell compartment. Although *Gli2* transgene expression is restricted to epithelial cells, we also detect striking alterations in bone adjacent to BSCCs, with activated osteoblasts, osteoclasts and osteal macrophages, indicative of active bone remodeling. *Gli2* transgene inactivation resulted in rapid BSCC regression and reversal of the bone remodeling phenotype. This first-reported mouse model of BSCC supports the concept that uncontrolled Hh signaling plays a central role in the pathogenesis of a subset of human BSCCs, points to Hh/GLI2 signaling as a potential therapeutic target and provides a powerful new tool for probing the mechanistic underpinnings of tumor-associated bone remodeling.

Received: March 11, 2021; **Revised:** May 17, 2021; **Accepted:** June 9, 2021

Graphical Abstract

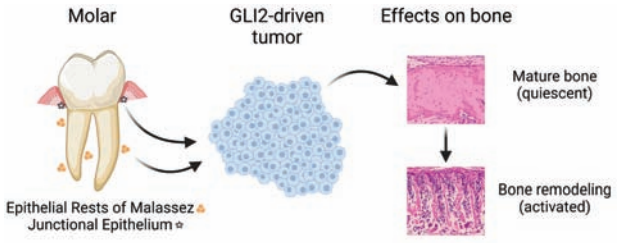

Basaloid squamous cell carcinoma development in mandibles and maxillae of GLI2-expressing mice. Tumors appear to arise from putative stem cells in the epithelial rests of Malassez or from gingival junctional epithelium and are associated with prominent bone remodeling. Extinguishing GLI2 expression leads to rapid tumor regression and reversion to normal-appearing bone histology (not shown). GLI2 signaling is active in a subset of human basaloid squamous cell carcinomas and may play a role in their development and progression.

Abbreviations

ACC	adenoid cystic carcinoma
BCC	basal cell carcinoma
BSCC	basaloid squamous cell carcinoma
H&E	hematoxylin and eosin
Hh	Hedgehog
PCNA	proliferating cell nuclear antigen
SCC	squamous cell carcinoma
SMA	smooth muscle actin

Introduction

Basal cell carcinoma (BCC), an extremely common skin tumor, was the first malignancy shown to be associated with aberrations in the Hedgehog (Hh) signaling pathway. Loss-of-function mutations affecting the Hh receptor/signaling repressor, PTCH1, were identified in patients with Gorlin's syndrome, who are at greatly increased risk for the development of BCC, and also in sporadic BCCs (1,2). Subsequent studies have shown that Hh signaling is deregulated in essentially all BCCs examined, due primarily to inactivating mutations in *PTCH1* or gain-of-function mutations affecting SMO, which is normally repressed by PTCH1. In both cases, intracellular Hh signaling is constitutively activated, leading to upregulation of Hh target genes due to activation of the GLI family of transcription factors. Several mouse models have confirmed the central role of deregulated Hh signaling in the pathogenesis of BCC (reviewed in ref. 3), and small-molecule Hh pathway inhibitors are effective in treating advanced and metastatic BCCs (4). In addition to BCC, several other types of tumors have been linked to defects in the Hh signaling pathway (5). Many of these cancers arise in target tissues, which rely on proper Hh signaling during embryogenesis or repair. Despite the role of Hh signaling in the formation of various head and neck structures, the potential involvement of the Hh pathway in repair, regeneration and pathology arising in this region is largely unexplored.

Although deregulated Hh signaling is associated with the development of human cancer, particularly BCC, relatively little attention has been focused on accompanying changes in surrounding tissues. The tumor microenvironment, comprising immune cells, fibroblasts and other stromal cells, blood vessels and extracellular matrix, is known to have an important role in tumor progression, metastasis and response to therapy (6). Complex interactions between tumor cells and the microenvironment not only have profound effects on tumorigenesis but can also alter neighboring tissues, such as bone (7).

In this report, we characterize basaloid squamous cell carcinomas (BSCCs), rare extracutaneous variants of squamous cell carcinoma (SCC) (8), arising in the jaws of 100% of mice engineered to reversibly over-express *Gli2* in squamous epithelia (9). We describe the biochemical and molecular features of these tumors, identify discreet cellular compartments from which they arise and establish a requirement for continued *Gli2* expression in maintenance of BSCC tumor cells. We also describe striking and yet reversible bone remodeling adjacent to growing BSCCs. The highly efficient induction of BSCCs in mice with upregulated Hh/GLI2 signaling, coupled with the discovery of inactivating *PTCH1* mutations in human BSCCs (10), points to a causal role for deregulated Hh signaling in BSCC tumorigenesis.

Materials and methods

Transgenic mice and transgene regulation

Generation of the *tetO-Gli2* construct, production of transgenic lines and generation of *K5-tTA;tetO-Gli2* double-transgenic mice were described previously (9). Three founders, *tetO-Gli2*^{446}, *tetO-Gli2*^{393}, and *tetO-Gli2*^{450}, yielded lines of mice that produced BCCs in skin as well as oral tumors. The *tetO-Gli2*^{446} line, which produced the most prominent phenotype, was used for the majority of studies presented in this report. Primers and PCR conditions for genotyping are available upon request. All mice were housed and maintained according to University of Michigan institutional guidelines, and protocols for mouse experiments were approved by the Institutional Animal Care and Use Committee.

In total, 34 *K5-tTA;tetO-Gli2* mice between the ages of 2 and 18 months were harvested from the three independent founder lines. For tumor regression experiments, 6–12-month-old tumor-bearing *K5-tTA;tetO-Gli2* mice and control littermates were treated with doxycycline to extinguish *Gli2* transgene expression. For the first 3 days, 20 mg/ml doxycycline was administered in drinking water with 5% sucrose together with doxycycline chow (Bio-serve, 200 mg/kg), which was continued for the time-period specified (typically 5–6 weeks). To assess potential tumor regrowth following doxycycline treatment, transgene was reactivated by transferring mice back to a regular chow diet for a 10–12 week period. Experimental and control mice were euthanized and tissue was collected for analysis.

Tissue collection

For analysis of tumors developing in the oral cavity of transgenic mice, intact heads were collected and fixed overnight in either neutral-buffered formalin or Bouin's solution, followed by decalcification in Cal-Ex II (Thermo Fisher Scientific, CA; CS5114D) at room temperature for 10 days, or in acetic acid/formal saline (11) at 4°C for 3 weeks. Tissue-containing vials were agitated on a rotating platform shaker for effective removal of calcium from bones and teeth, with decalcification solution replaced every 2–3 days. Mouse heads were bisected coronally and tissue was transferred to 70% ethanol, processed, embedded in paraffin, sectioned at 5 µm and used for hematoxylin and eosin (H&E) staining, immunostaining and *in situ* hybridization. De-identified sections of human tumor samples were obtained from the Rogel Cancer Center Tissue and Molecular Pathology Shared Resource, University of Michigan, for H&E staining and *in situ* hybridization. Data on previously sequenced tumors from the Michigan Oncology Sequencing Center (MI-ONCOSEQ), IRB Study ID: HUM00046018, were screened for tumors designated as 'basaloid squamous cell carcinoma', identifying one case.

In situ hybridization

In situ hybridization was performed on paraffin-embedded sections of neutral-buffered formalin- or Bouin's-fixed and decalcified tissue in an RNase free environment. Use of digoxigenin-labeled riboprobes allowed detection of Hh pathway target genes including mouse *Gli1* and *Ptch1*, human *GLI1*, *GLI2* and *PTCH1*, as well as a *Gli2* transgene-specific riboprobe designed to hybridize to the SV40 polyA sequence in *tetO-Gli2*. Detailed protocols and reagent sources for these probes are described elsewhere (12). The other probes used in this study included *Krt17* (13)

(provided by Pierre Coulombe, Johns Hopkins University, Baltimore, MD), *Ccnd1* and *Ccnd2* (14) (provided by Piotr Sicinski, Harvard Medical School, Boston, MA) and *Bcl2*, *Opn* and *Sfrp1*, which were designed to detect the corresponding mouse transcripts. A human-specific *KRT17* riboprobe was generated for *in situ* hybridization of human tumors. RNA isolated from mouse BCCs (15) or human keratinocytes was used as template for first strand synthesis using T3 or T7 promoters linked to specific PCR primers selected from the genes of interest. Primers for mouse *Bcl2* (forward 5′-gggaaacaccagaatcaagt-3′ and reverse 5′-agccaggagaaatcaaacag-3′), mouse *Opn* (forward 5′-cagccatgagtcaagtcagc-3′ and reverse 5′-ggccgtttgcatttcttgta-3′), mouse *Sfrp1* (forward 5′-gcggggccgcctcgggagtg-3′ and reverse 5′-agactggaaggtgggaca-3′) and human *KRT17* (forward 5′-gactcagtacaagaaagaacc-3′ and reverse 5′-tttaactgagtcaacaagc-3′) were selected to produce 818, 502, 961 and 268 base pair (bp) PCR fragments, respectively. These DNA PCR products were then used for *in vitro* transcription synthesis of the digoxigenin-uridine-5′-triphosphate-labeled riboprobes (via T3/T7 promoter sequences in PCR) for *in situ* hybridization (Roche Life Science).

Immunostaining

Bone-containing tissue samples fixed in Bouin's solution and paraffin-embedded were used for the majority of immunostaining. Neutral-buffered formalin-fixed tissue sections were deparaffinized and antigen retrieval was performed using boiling citrate-based buffer. Detailed protocols for immunostaining are described previously (12). The following antibodies and dilutions were used: anti-KRT1 and KRT5 (Covance, CA; 1:1000), KRT17 (13) (kindly provided by Pierre Coulombe; 1:1000), KRT10 (BioLegend, CA; 1:1000), proliferating cell nuclear antigen (PCNA; Thermo Fisher Scientific; 1:200), P63 (NeoMarkers, CA; 1:500), Sox9 (Millipore, CA; 1:1000), pSmad 1/5/8 (Cell Signaling, MA; 1:100), F4/80 (Cell Signaling; 1:250) and KRT14 and smooth muscle actin (SMA; NeoMarkers; 1:500, 1:1000, respectively). Primary antibodies were visualized using 3,3′-diaminobenzidine substrate following use of the Vectastain Peroxidase ABC Standard Kit (Vector Laboratories, CA; PK-4001), or the M.O.M. Kit (Vector Laboratories; PK-2200) as per manufacturer's directions with minor modifications. Slides were mounted with Permount mounting media (Thermo Fisher Scientific) following hematoxylin counterstain, and photographs taken on an Olympus BX51 microscope with Olympus DP74 camera system and cellSens Standard software.

Results

Fully penetrant BSCC development in *Gli2*-expressing mice

K5-tTA mice express a doxycycline-repressible transcriptional activator (tTA) in KRT5-positive epithelial basal cells, and *tetO-Gli2* mice carry a tTA-inducible *Gli2* transgene. Thus, *K5-tTA;tetO-Gli2* bitransgenic mice express *Gli2* in cells where the KRT5 promoter is active, and administration of doxycycline leads to efficient transgene inactivation (9). In addition to BCCs arising in skin, *K5-tTA;tetO-Gli2* mice also developed gross protrusions affecting the head (Figure 1A left panel). Although some lesions were jaw cysts similar to those we described in *K5-Gli2* single-transgenic mice and resembling human keratocysts associated with aberrant Hh signaling (11), analysis of sections from bitransgenic mice over 4 months of age revealed prominent epithelial tumors in the maxilla, mandible or nasopharynx in 100% of mice (n = 28) (Figure 1A right panel). Further examination of mice (n = 6) at ~2 months of age revealed the histological expansion of epithelial cells and presence of apparent nascent tumors in young mice.

Grossly apparent tumors, seen as early as 4 months of age, were detected in mice generated using three different *tetO-Gli2* mouse strains, ruling out transgene-related insertional mutagenesis as a contributing factor in tumor development. These tumors consisted largely of monomorphous basaloid cells with frequent mitoses, hyperchromatic nuclei, minimal cytoplasm, scattered foci of keratinization and regions of central necrosis (comedo necrosis) (Figure 1B left panels). These histological features are strikingly similar to those seen in human BSCC (Figure 1B right panels), a rare and aggressive high-grade variant of SCC first reported affecting the oral cavity, pharynx and larynx (16). *In situ* analysis of our mouse tumors revealed expression of mRNAs encoding the classical Hh target genes *Gli1* (Figure 1C) and *Ptch1* (Figure 1D), confirming activation of the Hh pathway in mouse tumor cells. Moreover, two out of five human BSCCs arising in the head and neck region also contained elevated levels of both *PTCH1* and *GLI1* mRNA (Figure 1C and D), at levels comparable with those seen in human BCCs arising in skin (Supplementary Figure S1A–C). These tumors also expressed *GLI2* mRNA at levels comparable with those seen in human BCCs as well as BCL2 protein (data not shown). In contrast, expression of Hh target genes *PTCH1* and *GLI1* was not detectably elevated in ameloblastoma, another odontogenic tumor of epithelial origin (Supplementary Figure S1A–D).

Biochemical and molecular characterization of mouse BSCCs

In situ analysis was performed to assess the expression of several additional genes in mouse *Gli2*-driven oral tumors. As expected, hybridization using a transgene-specific riboprobe

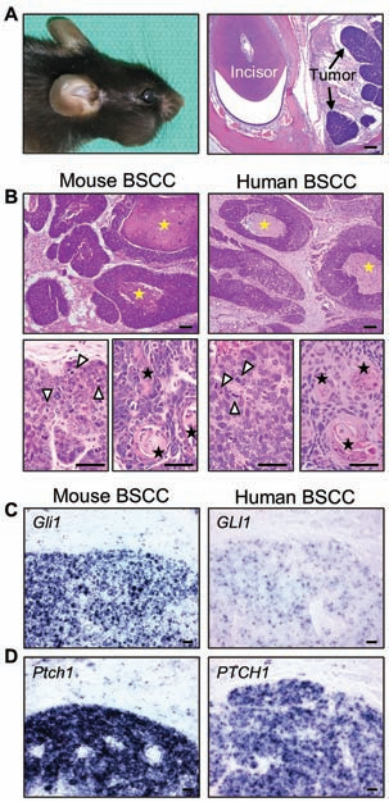

Figure 1. *Gli2*-driven oral tumors in mice resemble human BSCCs. (**A**) Gross abnormality in jaw of *K5-tTA;tetO-Gli2* mouse and H&E staining of representative tumor. Scale bar: 200 µm. (**B**) H&E staining of oral mouse tumors and human BSCC with regions of central necrosis (yellow stars), monomorphous basaloid cells with frequent mitoses (open arrowheads) and scattered foci of keratinization (black stars). Scale bars: 100 µm (upper panels) and 50 µm (lower panels). (**C** and **D**) *In situ* hybridization showing upregulation of Hh pathway target genes in mouse and human BSCCs. Scale bars: 20 µm.

revealed strong *Gli2* expression in tumor cells, focal expression in gingival epithelium and other sites where the KRT5 promoter is active, and no detectable expression in non-epithelial cells (Figure 2A). Upregulation of several other Hh-responsive genes, including *Ccnd1*, *Ccnd2*, *Bcl2* and *Sfrp1* (Figure 2B), was also detected. Notable, elevated expression of CCND1 (17) and BCL2 (18) protein has also been reported in human BSCCs. The well described dimorphic histopathological pattern of BSCCs, which includes a major basal cell component and associated foci of squamous differentiation, led us to examine the keratin expression pattern in *Gli2*-driven mouse tumors. The bulk of basaloid tumor cells expressed Keratin (KRT) 5 and KRT14 (Figure 2C), and cells located in keratinizing foci expressed the differentiation-specific keratins KRT1 and KRT10 (Figure 2D). As expected, the Hh pathway target gene KRT17 (19,20), which is consistently expressed in human and mouse BCCs, was highly expressed in these tumors (Figure 2E and Supplementary Figure S1D), as was SOX9 (Figure 2F), which is expressed in multiple cancers including BCCs (21). A high proliferative index, with the exception of differentiating cells in squamous foci, was confirmed by PCNA staining (Figure 2G). Mouse tumors were found to express p63 (Figure 2H) and lack SMA (Figure 2I), further reflecting the pattern observed in human BSCCs (22). Taken together with their distinctive histology, the molecular phenotype of *Gli2*-driven oral tumors is most consistent with a diagnosis of BSCC.

Localization of BSCC tumor progenitors

Analysis of tissue from relatively young animals (2 months of age) enabled us to examine early stages of BSCC tumor development in mice. Although the KRT5 promoter is active in the basal layer of epithelia throughout the oral cavity, nearly all early tumors were seen arising in one of three locations (see Supplementary Figure S2) including (i) the gingiva, (ii) epithelial rests of Malassez and (iii) the stratum intermedium of incisors. Tumors arising in the gingiva commonly appeared in the junctional epithelium, a compartment of cells immediately adjacent to molars (Figure 3A and Supplementary Figure S2). *In situ* hybridization for *Gli2* transgene and *Ptch1* (Figure 3B and C) as well as PCNA staining (Figure 3D) revealed Hh-pathway-driven tumor initiation particularly in this zone, suggesting this region contains potential tumor progenitors uniquely responsive to GLI2. A second site where tumors appeared was within the periodontal ligament, which anchors molar roots to the surrounding bone tissue. This site harbors a quiescent population of cells remaining after dissolution of the epithelial root called the epithelial rests of Malassez (23) (Figure 3E and Supplementary Figure S2). *Gli2* transgene expression and Hh pathway activation (*Ptch1*) in these previously dormant cells appear to be sufficient to stimulate their proliferation (Figure 3F–H right panels). Hh pathway activity, based on target gene expression, is undetectable in non-proliferative cells in control epithelial rests of Malassez (Figure 3F–H left panels). The third site of *Gli2*-driven oral tumors is the stratum intermedium (Figure 3I and Supplementary Figure 2), a population of supporting cells adjacent to the layer of ameloblasts, which continue to produce enamel in adult mice as incisors continue to grow throughout adulthood. The stratum intermedium is not present in humans since growth of incisors does not persist into adulthood. Regions of highly proliferative PCNA-positive basaloid hyperplasia and tumor foci were detected contiguous to and apparently arising from the stratum intermedium of *K5-tTA;tetO-Gli2* mice (Figure 3I and J).

Continuous *Gli2* expression/Hh signaling is required for BSCC tumor maintenance

Given the requirement for sustained Hh/GLI2 signaling in cutaneous BCCs (9), we examined the consequences of inactivating *Gli2* expression in established BSCCs. Transgene shutdown following doxycycline treatment led to tumor regression and formation of masses of keratinized material, with a small number of residual epithelial cells (Figure 4A). *In situ* hybridization showed loss of *Gli2* expression and transcripts encoding multiple Hh target genes, confirming effective transgene shutdown and consequent inhibition of Hh signaling (Figure 4B–F). Residual epithelial cells expressed KRT5 and KRT17, whereas some differentiated cells showed positivity for the differentiation marker KRT1 (Supplementary Figure S3A–C). PCNA was expressed in a small population of residual epithelial cells and surrounding stroma following transgene inactivation for 3 weeks (Supplementary Figure S3D). These data indicate that nearly all proliferative BSCC tumor cells, and therefore viable tumor mass, are dependent on continued *Gli2* expression, but the persistence of a small number of residual epithelial cells suggests that these cells may represent dormant tumor cells capable of re-initiating tumor growth if *Gli2* expression is reactivated. Doxycycline withdrawal, to reactivate transgene expression, indeed led to BSCC tumor regrowth (Supplementary Figure S4A–C), indicating that dormant cells capable of tumor regrowth do persist.

Gli2-driven BSCCs are associated with prominent bone remodeling

Although *Gli2* transgene expression is limited to epithelial cells in this model, prominent changes were also detected in other cell types in mice with odontogenic tumors. BSCC tumor stroma, in contrast to mesenchymal cells in the normal jaw, contained a large fraction of proliferating, PCNA-positive cells (data not shown). In addition, there were striking alterations in bone adjacent to BSCC tumors of *K5-tTA;tetO-Gli2* mice, which were fully reversible upon *Gli2* transgene inactivation (Figure 5). In contrast to the relatively quiescent cell populations detected in resting jaw bones of control mice, with characteristic flat-shaped bone lining cells (24) along the outer borders and differentiated osteocytes in the matrix, bone morphology was completely disrupted in areas adjacent to BSCCs. Affected bone in tumor-bearing mice exhibited finger-like projections with several distinctive bone remodeling cell populations infiltrating the region that were absent either in control mice or following *Gli2* inactivation (Figure 5C).

Affected bone in BSCC-bearing mice contained numerous cells with histological features of either osteoclasts or osteoblasts. Numerous large multi-nucleated ruffled cells, morphologically resembling osteoclasts, were observed along the periphery and invading affected bone nearest to BSCC tumors, whereas the population of cuboidal cells was presumably osteoblasts, which assume this shape only once activated (Figure 5C middle panel; Figure 6A and B). PCNA immunostaining indicated brisk proliferative activity in regions where bone remodeling was taking place (Figure 6C), which was particularly evident at the distal bone border but also included invading projections of cells into affected bone, possibly the sites of bone cell progenitors giving rise to activated cells involved in remodeling. In contrast, bone in control mice showed no proliferative activity with quiescent flat bone lining cells negative for PCNA staining (Figure 6D arrowheads). Additional staining for the macrophage marker F4/80 indicated the presence of a large number of non-osteoclast

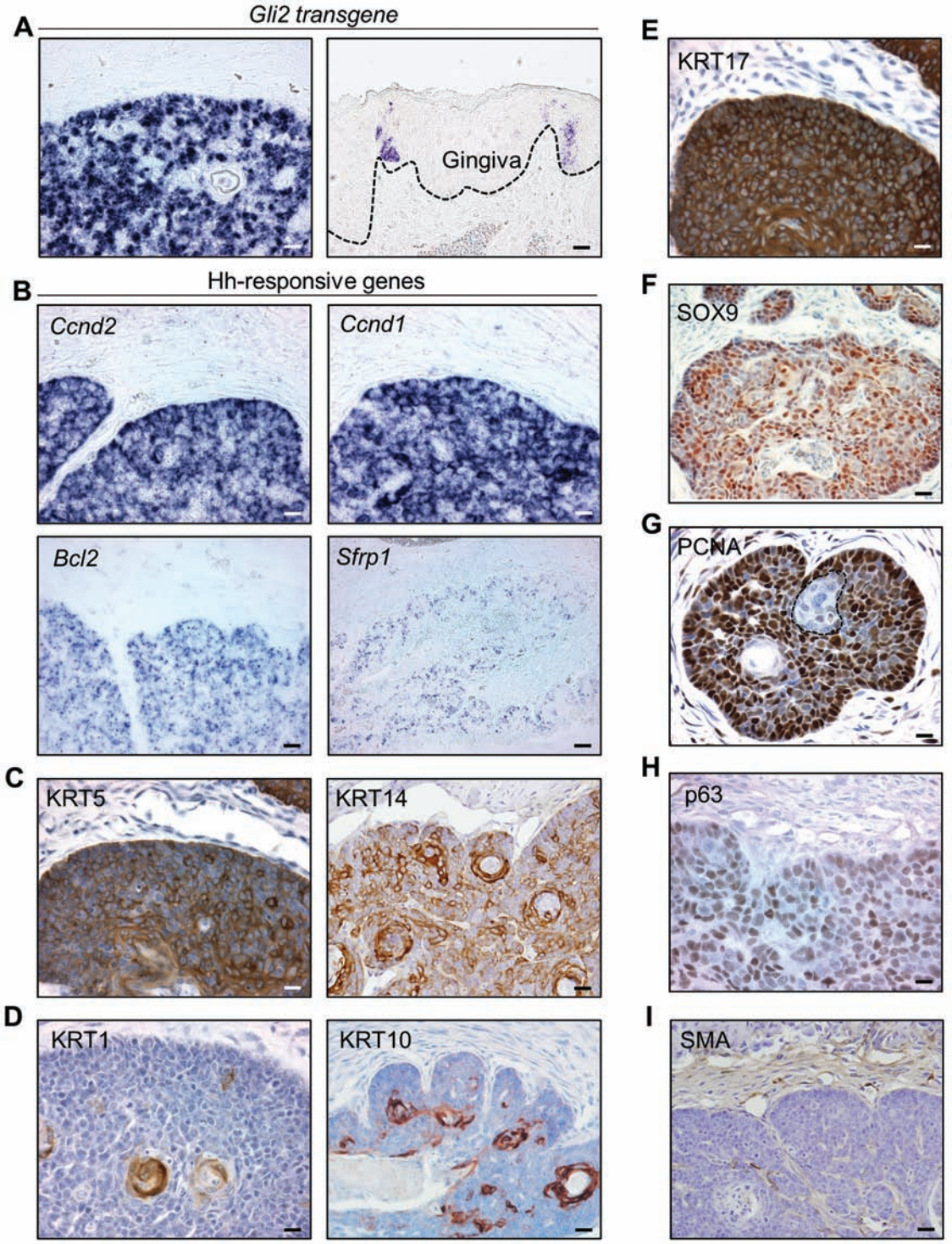

Figure 2. Molecular and biochemical characterization of mouse BSCCs. (**A**) *In situ* hybridization showing transgene expression in tumor cells and in focal regions of gingival epithelium. (**B**) Elevated expression of Hh target genes *Ccnd2*, *Ccnd1*, *Bcl2* and *Sfrp1* in mouse BSCCs. (**C–I**) Immunostaining for basal cell markers KRT5 and KRT14 (C), differentiation markers KRT1 and KRT10 (D), KRT17 (E), SOX9 (F), PCNA (G), p63 (H) and SMA (I) in BSCCs from *K5-tTA;tetO-Gli2* mice. All scale bars: 20 µm.

macrophages in affected bone of bitransgenic mice (Figure 6E). Notably, these osteal macrophages have been described located immediately adjacent to mature osteoblasts at sites of active bone remodeling (reviewed in ref. 25). Typical osteoclast populations were positive for pSMAD1/5/8 (Figure 6F), bone morphogenic protein signaling molecules required for osteoclast terminal differentiation (reviewed in ref. 26). Expression of mRNA encoding the bone matrix protein osteopontin (OPN) was confirmed by *in situ* hybridization in an expanded population of cells at the proximal tumor border and invading affected bone near the tumor nodules (Figure 6G). Osteoblasts in control tissue were present as morphologically distinct *Opn*-expressing flattened cells, suggesting they were not actively synthesizing bone (Figure 6H). Interestingly, although *Opn* is a Hh target gene

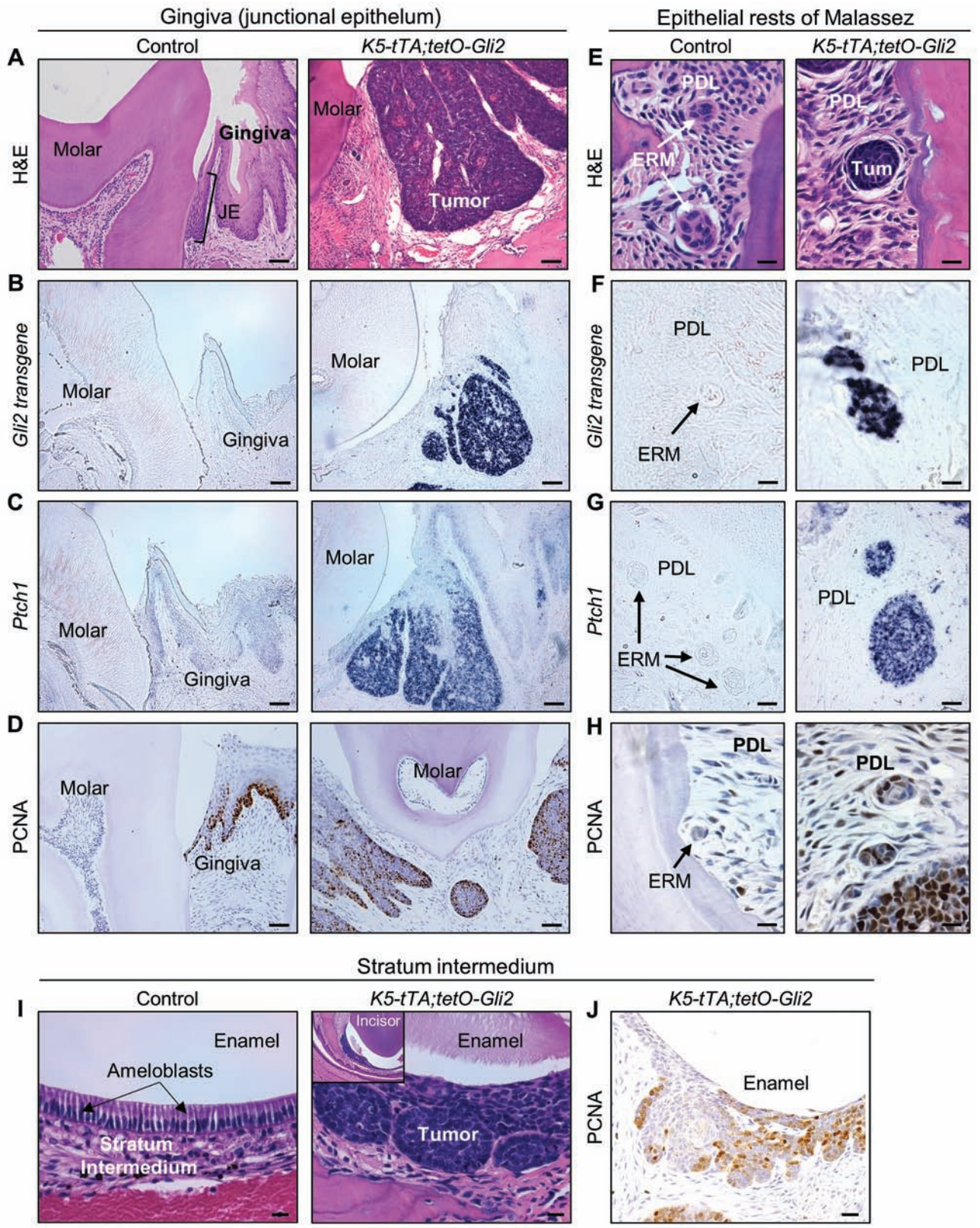

Figure 3. Sites of early-stage BSCC development in *K5-tTA;tetO-Gli2* mice. (**A–D**) H&E staining showing molar with junctional epithelium (JE) of gingiva in control mouse and gingiva-derived tumor in *K5-tTA;tetO-Gli2* mouse (A). Corresponding *in situ* hybridization for *Gli2* transgene (B) and *Ptch1* (C), as well as immunostaining for PCNA (D). Scale bars: 50 μm. (**E–H**) H&E staining of mouse epithelial rests of Malassez (ERM) (E) (see also Supplementary Figure S2) within the periodontal ligament (PDL) in jaws of control and *K5-tTA;tetO-Gli2* mice. *In situ* hybridization for *Gli2* transgene (F) and *Ptch1* (G) as well as immunostaining for PCNA (H) in control ERM and ERM-derived tumors. Scale bars: 20 μm. (**I** and **J**) H&E staining of mouse incisor illustrating ameloblasts and adjacent stratum intermedium layer in control mice, and tumors arising in *K5-tTA;tetO-Gli2* mice (I). Inset shows tumor location at lower magnification. Immunostaining for PCNA (J) indicates proliferative activity. Scale bars: 20 μm. PDL, periodontal ligament; ERM, epithelial rests of Malassez.

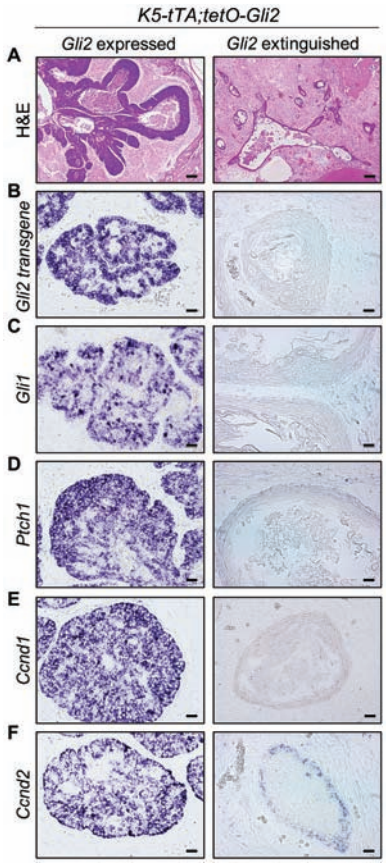

Figure 4. GLI2 expression/Hh signaling is required for BSCC tumor maintenance. (**A**) H&E staining of BSCCs with *Gli2* transgene expressed (left panel) versus residual epithelial cells when transgene is extinguished (right panel) by doxycycline administration. Scale bars: 200 µm. (**B–F**) *In situ* hybridization showing expression of *Gli2* transgene (B) and target genes (C–F) in tumor cells and residual cells following tumor regression. Scale bars: 20 µm.

(27,28), we did not detect increased expression in murine BSCC tumor cells (data not shown).

Discussion

BSCC is a rare but distinctive variant of SCC typically presenting in the upper aerodigestive tract including the esophagus, oral cavity and other head and neck structures including the maxilla (29–33). Multiple potential oncogenic drivers of esophageal BSCC development have been described (reviewed in ref. 34), including mutations of the Hh pathway tumor suppressor gene *PTCH1* (10). Upregulation of Hh target genes in two out of five human BSCCs that we examined identifies constitutive Hh signaling in a subset of BSCCs; moreover, the highly penetrant development of BSCCs in our *Gli2*-expressing mouse model suggests that oncogenic activation of the Hh pathway may operate as an oncogenic driver for BSCC tumorigenesis.

Although histologically distinct, BSCC tumors can be difficult to distinguish from other malignant tumors including small cell undifferentiated carcinoma, adenoid cystic carcinoma (ACC), neuroendocrine carcinoma, adenosquamous carcinoma, basal cell adenocarcinoma and salivary duct carcinoma (30,35). Presence or absence of ductal structures and squamous components can aid in the differential diagnosis, which is critical since prognosis and therapeutic options differ among these tumor types. KRT14, which was present in our oral mouse tumors (Figure 2C), is typically not observed in small cell undifferentiated carcinoma or neuroendocrine tumors (36,37). ACC has the strongest histological resemblance and a relatively similar marker profile as BSCC (30,36,38). However, key features including high mitotic rate, nuclear pleomorphism and comedonecrosis are typically considered more prominent in BSCC than ACC (36,39,40). Additionally, expression of the p53 family member p63 in nearly all cells of human BSCC tumor cells is distinct from the compartmentalized pattern typically seen at the periphery of tumor nests in high-grade ACC (41). Murine *Gli2*-driven BSCCs express p63 diffusely (Figure 2H), reflecting the pattern in human BSCCs (22). Furthermore, ACC is typically positive for SMA, whereas BSCC is negative (42,43), as observed in our oral mouse tumors (Figure 2I). Taken together with their distinctive histology, the immunophenotype of *Gli2*-driven oral tumors is thus most consistent with a BSCC diagnosis.

To investigate the link between deregulated Hh signaling in tumors arising in our *Gli2* mouse model and human basaloid SCCs, we additionally analyzed five patient tumor samples. Since activity of the Hh pathway is limited to a small number of cells in most adult organs, finding high levels of Hh target gene expression in these samples would strongly suggest that this pathway has been pathologically activated, either by mutation of key regulatory genes or by reactivation of Hh ligand expression. Two of the five human BSCCs we examined contained elevated levels of both *PTCH1* and *GLI1* (Figure 1C and D). Although limited to a small cohort, upregulation of Hh target gene expression provides independent evidence supporting a link between Hh signaling and the pathogenesis of at least a subset of human BSCCs. In light of our findings, it is noteworthy that inactivating mutations in *PTCH1* were identified in 53.3% of esophageal BSCCs (10), providing a potential mechanism for Hh pathway deregulation in these tumors. Furthermore, retrospective review of the Michigan Oncology Sequencing Center (MI-ONCOSEQ) tumor sequencing database identified one BSCC with GLI2 amplification (data not shown). Combined with our findings that GLI2 expression is sufficient to drive BSCC development in mice, these data suggest that blockade of Hh signaling at the level of GLI transcription factors may provide a novel approach to treating Hh-pathway-activated BSCCs.

Little is known about the potential cells of origin of human BSCC. Here, we show that *Gli2*-driven mouse BSCCs can arise from distinct populations in the (i) gingival epithelium, (ii) epithelial rests of Malassez and (iii) stratum intermedium (Figure 3 and Supplementary Figure S2). The majority of tumors arose in the gingival junctional epithelium (Figure 3A–D), suggesting this site contains a unique population of tumor progenitors competent to respond to oncogenic GLI2 signals. Interestingly, this is also the site where chemically induced squamous cell tumors first arise in rats (44), suggesting that it harbors progenitor cells capable of giving rise to both squamous and basaloid tumors of the oral cavity. Tumors also arose from the epithelial rests of Malassez (Figure 3E–H), a quiescent population of cells proposed to have stem cell properties (45,46), which we have shown previously can be reactivated to proliferate and differentiate to yield odontogenic keratocysts (11). These data reveal that BSCCs in *Gli2*-expressing mice may arise either directly from the gingival epithelium (particularly the junctional epithelium), from dormant epithelial rests within the periodontal ligament or occasionally from the stratum intermedium, suggesting that

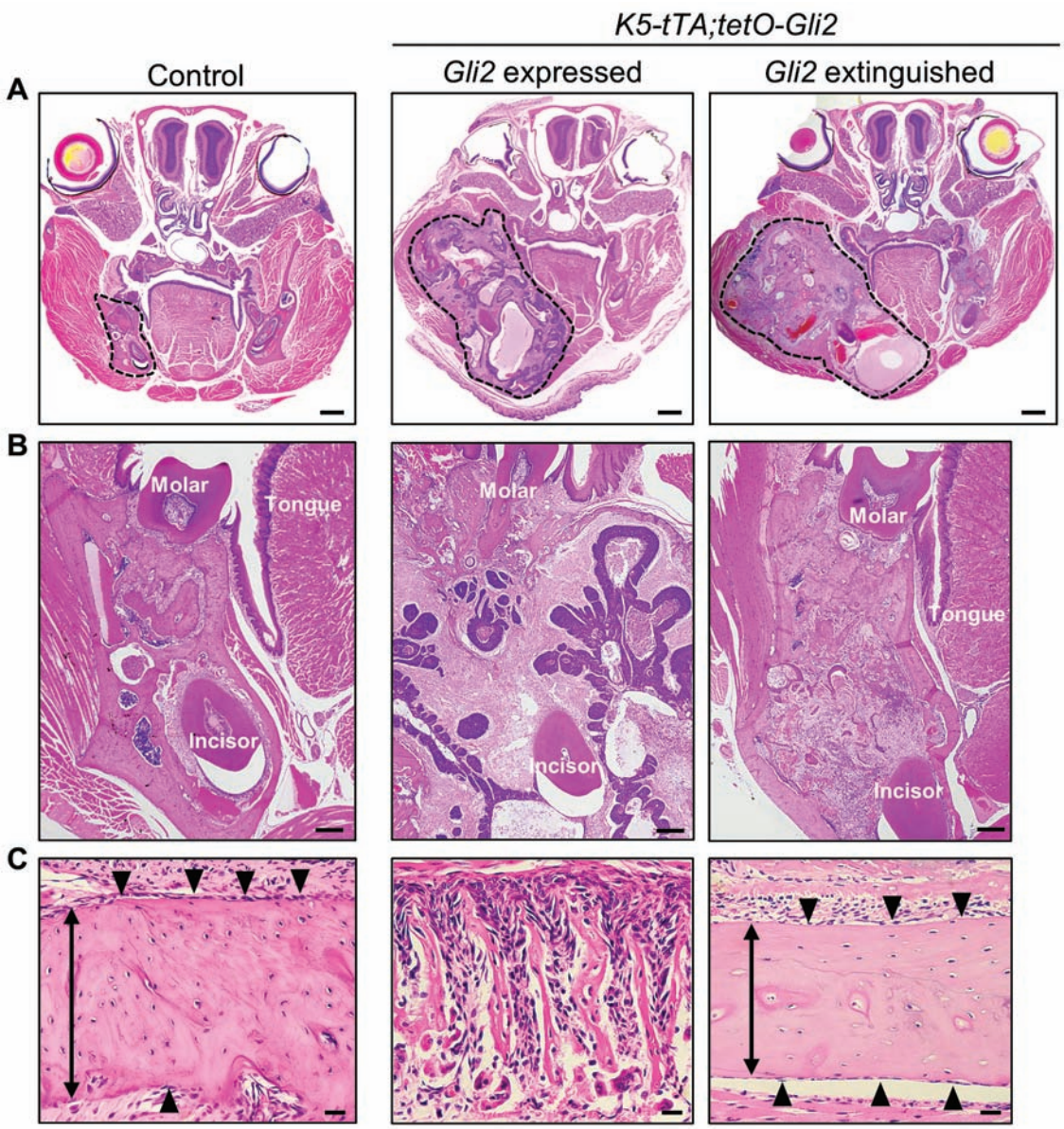

Figure 5. Reversible bone remodeling associated with *Gli2*-driven BSCCs. (**A** and **B**) H&E stained coronal sections of mouse heads from control and *K5-tTA;tetO-Gli2* mice with GLI2 expressed or extinguished, which leads to loss of proliferating tumor cells. Note that despite tumor regression, structure of the head remains grossly deformed. Scale bars: 500 μm (A) and 200 μm (B). (**C**) H&E staining of bone from control and *K5-tTA;tetO-Gli2* mice. Note similar histology of bone from control and GLI2 extinguished *K5-tTA;tetO-Gli2* mouse, in contrast to the highly cellular, activated bone remodeling phenotype in tumor-bearing GLI2-expressing *K5-tTA;tetO-Gli2* mouse (see also Figure 6). Mature bone thickness in control and GLI2 extinguished bitransgenic mice is marked with double-headed arrows and single layers of flat bone lining cells are shown with arrowheads. Scale bars: 20 μm.

several distinct cell populations can give rise to histologically similar tumors in response to deregulated Hh signaling in the oral cavity.

Interestingly, striking alterations in bone morphology were identified directly adjacent to BSCC tumors arising in the oral cavity of *K5-tTA;tetO-Gli2* mice (Figure 5). This complete disruption of bone morphology was reversed upon *Gli2* transgene inactivation and tumor regression (Figure 5C). Deregulated homeostatic bone remodeling, which involves a balance of bone resorption by osteoclasts and formation of new bone matrix by osteoblasts, is an established consequence of many pathological conditions including local tumor invasion, progression and metastasis. Local bone invasion by oral SCCs has been described (47) and may be associated with an increase in both osteoclastic and osteoblastic activity. More recently, BSCC causing extensive bone destruction has also been reported (48). Affected bone in BSCC-bearing mice contained numerous cells with histological features of either activated cuboidal osteoblasts or osteoclasts (Figure 6A). Although osteoclasts are relatively rare and difficult to detect in resting bone, numerous large multi-nucleated ruffled cells, morphologically resembling osteoclasts, were observed along the periphery and invading into affected bone nearest to tumors (Figure 6A and B). This is reminiscent of previously described oral carcinomas driving bone destruction by osteoclasts pushing ahead of the advancing tumor, often associated with an erosive histological pattern (49,50).

In this study, we describe a doxycycline-regulated mouse model showing that (i) Hh/GLI2 signaling is sufficient to drive

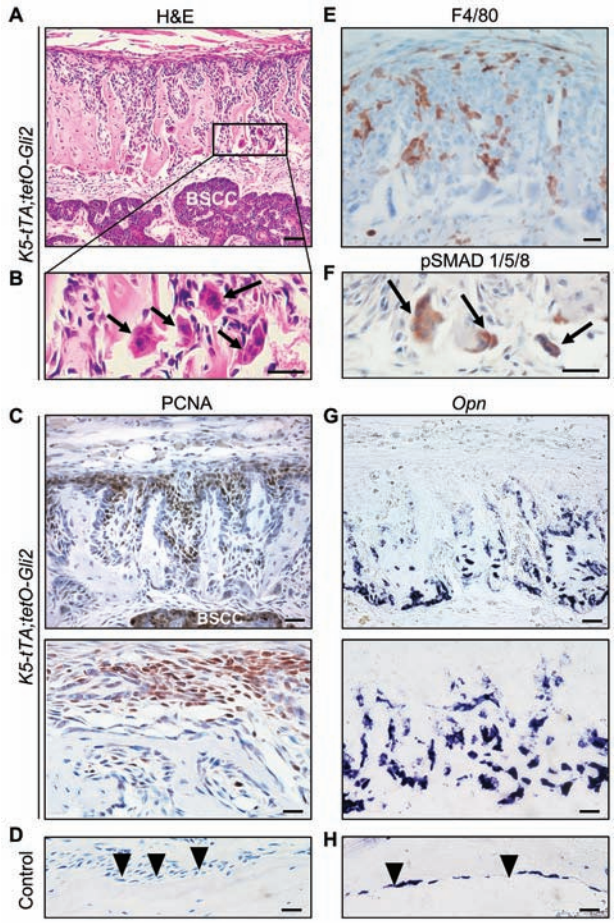

Figure 6. Activation of bone cells neighboring *Gli2*-driven mouse BSCCs. (**A**) H&E staining of oral region showing affected bone tissue, neighboring BSCCs and stromal cells in *K5-tTA;tetO-Gli2* mice. Scale bars: 50 µm. (**B**) Inset highlights multi-nucleated giant bone cells (arrows) consistent with activated osteoclasts. Scale bar: 20 µm. (**C** and **D**) Immunostaining for proliferative marker PCNA in *K5-tTA;tetO-Gli2* (C) and control (D) mice. PCNA-positive cells are present in BSCC tumors as well as in affected bone regions of *K5-tTA;tetO-Gli2* mice, whereas absent in flat cells lining bone of control mice (arrowheads). Lower panel in (C) depicts typical appearance of upper panel at higher magnification. Scale bars: 50 and 20 µm, respectively. (**E**) Immunostaining for F4/80 illustrates presence of macrophages in areas with active bone remodeling. Scale bar: 20 µm. (**F**) Immunostaining for pSMAD 1/5/8 in multi-nucleated, giant bone cells. Scale bars: 20 µm. (**G** and **H**) *In situ* hybridization staining for *Osteopontin* (*Opn*) in jaw bone of *K5-tTA;tetO-Gli2* (G) and control (H) mice. Upper panel (G) denotes a representative region shown below at higher magnification. Note the morphological difference in *Osteopontin*-positive cells in *K5-tTA;tetO-Gli2* mice compared with cells in controls (arrowheads). Scale bars: 50 and 20 µm, respectively. PDL: periodontal ligament.

fully penetrant mouse BSCC development, (ii) sustained GLI2 expression is required for tumor maintenance and (iii) GLI2-driven BSCCs stimulate dramatic remodeling of bone adjacent to tumors. In contrast to Hh-driven human BCCs, which are extremely common, develop only in skin and are typically cured by surgery, BSCCs rarely arise in skin and may have an aggressive clinical course. In addition to yielding insights into the biology and potential molecular basis of BSCC, this model provides a powerful new tool for exploring pathways underlying tumor-associated bone remodeling and may ultimately help uncover novel therapies.

Supplementary material

Supplementary data are available at *Carcinogenesis* online.

Funding

National Institutes of Health (CA087837 and CA118875 to A.A.D.); Helen L. Kay Charitable Trust; Rogel Cancer Center Support Grant (CA046592).

Acknowledgements

We thank members of the Dlugosz laboratory for constructive comments on the manuscript. We are grateful to Pierre Coulombe, Adam Glick, Piotr Sicinski, John Foley, Laurie McCauley, Renny Franceschi and Evan Keller for providing reagents and/or mice and helpful discussions; the personnel in the University of Michigan Transgenic Model Core for production of *tetO-Gli2* founders; the Rogel Cancer Center Tissue and Molecular Pathology Shared Resource, including Thomas Giordano, Department of Pathology, for access to de-identified archival human paraffin blocks; and Janice Berry for assistance with *in situ* analysis. We gratefully acknowledge Donna Albertson, Antoine Snijders, Ian Mackenzie, Kurt Hankenson, Muhammed Kariapper, Evan Michael and Nisha D'Silva for helpful discussions. The graphical abstract was created with BioRender.com.

Conflict of Interest Statement: None declared.

References

1. Hahn, H. *et al*. (1996) Mutations of the human homolog of *Drosophila* patched in the nevoid basal cell carcinoma syndrome. *Cell*, 85, 841–851.

2. Johnson, R.L. *et al.* (1996) Human homolog of patched, a candidate gene for the basal cell nevus syndrome. *Science*, 272, 1668–1671.
3. Kasper, M. *et al.* (2012) Basal cell carcinoma—molecular biology and potential new therapies. *J. Clin. Invest.*, 122, 455–463.
4. Danhof, R. *et al.* (2018) Small molecule inhibitors of the Hedgehog pathway in the treatment of basal cell carcinoma of the skin. *Am J Clin Dermatol.*, 19, 195–207.
5. Barakat, M.T. *et al.* (2010) Learning from Jekyll to control Hyde: Hedgehog signaling in development and cancer. *Trends Mol. Med.*, 16, 337–348.
6. Valkenburg, K.C. *et al.* (2018) Targeting the tumour stroma to improve cancer therapy. *Nat. Rev. Clin. Oncol.*, 15, 366–381.
7. Olechnowicz, S.W. *et al.* (2014) Contributions of the host microenvironment to cancer-induced bone disease. *Cancer Res.*, 74, 1625–1631.
8. Fritsch, V.A. *et al.* (2013) Basaloid squamous cell carcinoma of the oropharynx: an analysis of 650 cases. *Otolaryngol. Head Neck Surg.*, 148, 611–618.
9. Hutchin, M.E. *et al.* (2005) Sustained Hedgehog signaling is required for basal cell carcinoma proliferation and survival: conditional skin tumorigenesis recapitulates the hair growth cycle. *Genes Dev.*, 19, 214–223.
10. Saito, T. *et al.* (2015) PTCH1 mutation is a frequent event in oesophageal basaloid squamous cell carcinoma. *Mutagenesis*, 30, 297–301.
11. Grachtchouk, M. *et al.* (2006) Odontogenic keratocysts arise from quiescent epithelial rests and are associated with deregulated hedgehog signaling in mice and humans. *Am. J. Pathol.*, 169, 806–814.
12. Grachtchouk, V. *et al.* (2003) The magnitude of hedgehog signaling activity defines skin tumor phenotype. *EMBO J.*, 22, 2741–2751.
13. McGowan, K.M. *et al.* (1998) Onset of keratin 17 expression coincides with the definition of major epithelial lineages during skin development. *J. Cell Biol.*, 143, 469–486.
14. Ciemerych, M.A. *et al.* (2002) Development of mice expressing a single D-type cyclin. *Genes Dev.*, 16, 3277–3289.
15. Grachtchouk, M. *et al.* (2000) Basal cell carcinomas in mice overexpressing Gli2 in skin. *Nat. Genet.*, 24, 216–217.
16. Wain, S.L. *et al.* (1986) Basaloid-squamous carcinoma of the tongue, hypopharynx, and larynx: report of 10 cases. *Hum. Pathol.*, 17, 1158–1166.
17. Cho, K.J. *et al.* (2017) Basaloid squamous cell carcinoma of the head and neck: subclassification into basal, ductal, and mixed subtypes based on comparison of clinico-pathologic features and expression of p53, cyclin D1, epidermal growth factor receptor, p16, and human papillomavirus. *J. Pathol. Transl. Med.*, 51, 374–380.
18. Sarbia, M. *et al.* (1999) Expression of Bcl-2 and amplification of c-myc are frequent in basaloid squamous cell carcinomas of the esophagus. *Am. J. Pathol.*, 155, 1027–1032.
19. Callahan, C.A. *et al.* (2004) MIM/BEG4, a sonic hedgehog-responsive gene that potentiates Gli-dependent transcription. *Genes Dev.*, 18, 2724–2729.
20. Bianchi, N. *et al.* (2005) Exploiting the keratin 17 gene promoter to visualize live cells in epithelial appendages of mice. *Mol. Cell. Biol.*, 25, 7249–7259.
21. Vidal, V.P. *et al.* (2008) SOX9 expression is a general marker of basal cell carcinoma and adnexal-related neoplasms. *J. Cutan. Pathol.*, 35, 373–379.
22. Emanuel, P. *et al.* (2005) p63 immunohistochemistry in the distinction of adenoid cystic carcinoma from basaloid squamous cell carcinoma. *Mod. Pathol.*, 18, 645–650.
23. Yang, Z. *et al.* (2015) Role of the epithelial cell rests of Malassez in periodontal homeostasis and regeneration—a review. *Curr. Stem Cell Res. Ther.*, 10, 398–404.
24. Florencio-Silva, R. *et al.* (2015) Biology of bone tissue: structure, function, and factors that influence bone cells. *Biomed Res. Int.*, 2015, 421746.
25. Sinder, B.P. *et al.* (2015) Macrophages: their emerging roles in bone. *J. Bone Miner. Res.*, 30, 2140–2149.
26. Huntley, R. *et al.* (2019) Bone morphogenetic proteins: their role in regulating osteoclast differentiation. *Bone Rep.*, 10, 100207.
27. Yoon, J.W. *et al.* (2002) Gene expression profiling leads to identification of GLI1-binding elements in target genes and a role for multiple downstream pathways in GLI1-induced cell transformation. *J. Biol. Chem.*, 277, 5548–5555.
28. Das, S. *et al.* (2009) The hedgehog pathway transcription factor GLI1 promotes malignant behavior of cancer cells by up-regulating osteopontin. *J. Biol. Chem.*, 284, 22888–22897.
29. Schuch, L.F. *et al.* (2020) Basaloid squamous cell carcinoma: a 31-year retrospective study and analysis of 214 cases reported in the literature. *Oral Maxillofac. Surg.*, 24, 103–108.
30. Wieneke, J.A. *et al.* (1999) Basaloid squamous cell carcinoma of the sinonasal tract. *Cancer*, 85, 841–854.
31. Gupta, B. *et al.* (2018) Basaloid squamous cell carcinoma—a rare and aggressive variant of squamous cell carcinoma: a case report and review of literature. *Natl. J. Maxillofac. Surg.*, 9, 64–68.
32. Kuan, E.C. *et al.* (2015) Basaloid squamous cell carcinoma of the maxilla: report of a case and literature review. *Am. J. Otolaryngol.*, 36, 402–407.
33. Jumaily, M. *et al.* (2019) Basaloid squamous cell carcinoma of the larynx: a National Cancer Database analysis. *Otolaryngol. Head Neck Surg.*, 160, 847–854.
34. Saito, T. *et al.* (2015) Molecular pathology and potential therapeutic targets in esophageal basaloid squamous cell carcinoma. *Int. J. Clin. Exp. Pathol.*, 8, 2267–2273.
35. Franchi, A. *et al.* (2011) Current diagnostic strategies for undifferentiated tumours of the nasal cavities and paranasal sinuses. *Histopathology*, 59, 1034–1045.
36. Coletta, R.D. *et al.* (2002) Basaloid squamous carcinoma of oral cavity: a histologic and immunohistochemical study. *Oral Oncol.*, 38, 723–729.
37. Sturm, N. *et al.* (2001) Thyroid transcription factor 1 and cytokeratins 1, 5, 10, 14 (34betaE12) expression in basaloid and large-cell neuroendocrine carcinomas of the lung. *Hum. Pathol.*, 32, 918–925.
38. Tsang, W.Y. *et al.* (1991) Basaloid-squamous carcinoma of the upper aerodigestive tract and so-called adenoid cystic carcinoma of the oesophagus: the same tumour type? *Histopathology*, 19, 35–46.
39. Barnes, L. *et al.* (1996) Basaloid squamous cell carcinoma of the head and neck: clinicopathological features and differential diagnosis. *Ann. Otol. Rhinol. Laryngol.*, 105, 75–82.
40. Ferlito, A. *et al.* (1997) Basaloid squamous cell carcinoma of the larynx and hypopharynx. *Ann. Otol. Rhinol. Laryngol.*, 106, 1024–1035.
41. Emanuel, P. *et al.* (2005) p63 immunohistochemistry in the distinction of adenoid cystic carcinoma from basaloid squamous cell carcinoma. *Mod. Pathol.*, 18, 645–650.
42. Morice, W.G. *et al.* (1998) Distinction of basaloid squamous cell carcinoma from adenoid cystic and small cell undifferentiated carcinoma by immunohistochemistry. *Hum. Pathol.*, 29, 609–612.
43. Klijanienko, J. *et al.* (1993) Basaloid squamous carcinoma of the head and neck. Immunohistochemical comparison with adenoid cystic carcinoma and squamous cell carcinoma. *Arch. Otolaryngol. Head Neck Surg.*, 119, 887–890.
44. Yoshizawa, K. *et al.* (2005) Gingival carcinogenicity in female Harlan Sprague–Dawley rats following two-year oral treatment with 2,3,7,8-tetrachlorodibenzo-*p*-dioxin and dioxin-like compounds. *Toxicol. Sci.*, 83, 64–77.
45. Padma Priya, S. *et al.* (2015) Odontogenic epithelial stem cells: hidden sources. *Lab. Invest.*, 95, 1344–1352.
46. Athanassiou-Papaefthymiou, M. *et al.* (2015) Isolation and characterization of human adult epithelial stem cells from the periodontal ligament. *J. Dent. Res.*, 94, 1591–1600.
47. Jimi, E. *et al.* (2011) The cellular and molecular mechanisms of bone invasion by oral squamous cell carcinoma. *Oral Dis.*, 17, 462–468.
48. Al Feghali, K.A. *et al.* (2015) Basaloid squamous cell carcinoma of the ethmoid sinus with invasion into the skull base treated with craniofacial resection and adjuvant intensity-modulated radiation therapy: a case report. *Cureus*, 7, e421.
49. Carter, R.L. (1980) Direct bone invasion by squamous carcinomas of the head and neck. *Clin. Otolaryngol. Allied Sci.*, 5, 85–86.
50. Jimi, E. *et al.* (2013) The RANKL/RANK system as a therapeutic target for bone invasion by oral squamous cell carcinoma (Review). *Int. J. Oncol.*, 42, 803–809.